Low Cloud–SST Feedback over the Subtropical Northeast Pacific and the Remote Effect on ENSO Variability

LIU YANG, a.b.c.d SHANG-PING XIE, b SAMUEL S. P. SHEN, c.b JING-WU LIU, a AND YEN-TING HWANGE

^a Physical Oceanography Laboratory, Qingdao Collaborative Innovation Center of Marine Science and Technology, Ocean–Atmosphere Interaction and Climate Laboratory, Ocean University of China, Qingdao, China

^b Scripps Institution of Oceanography, University of California, San Diego, La Jolla, California

^c Department of Mathematics and Statistics, San Diego State University, San Diego, California

^d College of Aviation Meteorology, Civil Aviation Flight University of China, Guanghan, China ^e Department of Atmospheric Sciences, National Taiwan University, Taipei, Taiwan

(Manuscript received 26 November 2021, in final form 16 September 2022)

ABSTRACT: Low clouds frequent the subtropical northeastern Pacific Ocean (NEP) and interact with the local sea surface temperature (SST) to form positive feedback. Wind fluctuations drive SST variability through wind–evaporation–SST (WES) feedback, and surface evaporation also acts to damp SST. This study investigates the relative contributions of these feedbacks to NEP SST variability. Over the summer NEP, the low cloud–SST feedback is so large that it exceeds the evaporative damping and amplifies summertime SST variations. The WES feedback causes the locally enhanced SST variability to propagate southwestward from the NEP low cloud deck, modulating El Niño–Southern Oscillation (ENSO) occurrence upon reaching the equator. As a result, a second-year El Niño tends to occur when there are significant warm SST anomalies over the subtropical NEP in summer following an antecedent El Niño event and a second-year La Niña tends to occur when there are significant cold SST anomalies over the subtropical NEP in summer following an antecedent La Niña event The mediating role of the NEP low cloud–SST feedback is confirmed in a cloud-locking experiment with the Community Earth System Model, version 1 (CESM1). When the cloud–ocean coupling is disabled, SST variability over the NEP weakens and the modulating effect on ENSO vanishes. The nonlocal effect of the NEP low cloud–SST feedback on ENSO has important implications for climate prediction.

KEYWORDS: Air-sea interaction; Clouds; ENSO

1. Introduction

Low clouds over the eastern subtropical oceans play an important role in the local and large-scale sea surface temperature (SST) variability because their interaction yields positive feedback (Norris and Leovy 1994; Tanimoto and Xie 2002; Clement et al. 2009; Evan et al. 2013; Yuan et al. 2016; Bellomo et al. 2014, 2016; Brown et al. 2016). These clouds reflect incoming solar radiation and cool the underlying sea surface. The surface cooling increases the lower atmospheric stability in favor of low cloud formation. While the low cloud–SST feedback over the northeastern Pacific Ocean (NEP) is well known, its effect relative to other feedbacks is not well quantified, and the role in driving tropical SST variability deserves investigation.

Surface evaporation is a major process for the ocean to balance the incoming solar radiation and to heat the atmosphere. Latent heat flux is often represented with a bulk formula (Fairall et al. 1996, 2003), which can be decomposed into a thermodynamic term (sea-air specific humidity gradient) and wind speed term (Xie 1999). Variability in the sea-air humidity gradient and the surface wind speed can both change surface evaporation but their effects on SST are distinct. With a positive SST anomaly (SSTA), the sea-air humidity gradient and surface evaporation increase, and with a negative anomaly they decrease. This forms negative feedback on SST. The

trade wind anomalies over the subtropical NEP can force the SST variations by modifying surface evaporation, known as wind-evaporation-SST (WES) feedback (Xie and Philander 1994; Xie 1999). As such, the effects of sea-air humidity gradient feedback and the WES feedback on the local SST variability should be examined separately. It is unclear which of the humidity gradient feedback, WES feedback, and low cloud-SST feedback is the most important to the SST variability over the subtropical NEP.

The Pacific meridional mode (PMM; Chiang and Vimont 2004) develops during boreal winter because of the weakened North Pacific trade winds, forcing anomalous latent heat flux and warm SSTAs. These SSTAs extend from the coast of Baja California southwestward into the tropics during spring through WES feedback and persist into boreal summer, known as the seasonal footprinting mechanism (Vimont et al. 2001, 2003a,b). This ultimately drives atmospheric circulation anomalies in the deep tropics, triggering El Niño-Southern Oscillation (ENSO) (Vimont et al. 2003a,b, 2009; Amaya et al. 2019). The PMM has a large SSTA loading in the NEP low cloud deck region. Previous studies on PMM describe clouds as local feedback and mainly emphasize the role of WES feedback in the PMM modulation of ENSO (Vimont et al. 2001, 2003a,b). However, recent observational and modeling studies show that low cloud-SST feedback can sustain and enhance SSTAs over the midlatitude oceans, thus amplifying this subtropical meridional-mode-like SST variability (Smirnov and Vimont 2012; Bellomo et al. 2014, 2015; Myers et al. 2017, 2018b; Middlemas et al. 2019). While the low cloud-SST

Corresponding author: Shang-Ping Xie, sxie@ucsd.edu

feedback over the subtropical NEP appears to be important for North Pacific SST variability, it remains unclear whether the feedback contributes to the ENSO variability.

Pioneering studies in the 1990s (Klein and Hartmann 1993; Klein et al. 1995; Norris and Leovy 1994; Norris et al. 1998) relied heavily on shipboard observations, which are sparse in low cloud regions such as the southeastern Pacific. Satellite observations of solar radiation have expanded in frequency and time period and physically consistent atmospheric reanalyses have become widely available. The present study revisits NEP low cloud–SST feedback by using these extended data. We quantitatively compare the summertime low cloud–SST feedback with surface evaporation feedbacks to investigate the dominate process in affecting SST variability over the NEP low cloud region.

Long observation records enable us to identify a nonlocal effect of the NEP low cloud–SST feedback on ENSO, especially the so-called 2-yr events. Recent studies have shown that some El Niño and La Niña events can persist throughout the next year and reintensify in the following winter, identified as 2-yr El Niño and La Niña events (Horii and Hanawa 2004; Ohba and Ueda 2009; Okumura and Deser 2010; Lee et al. 2014; DiNezio et al. 2017; Okumura 2019; Wu et al. 2019, 2021; Jong 2020; Yu and Fang 2018; Fang and Yu 2020). We use 60-yr-long reanalysis products to examine the remote effect of subtropical NEP low cloud–SST feedback on tropical climate. We show that the NEP low cloud–SST feedback modulates ENSO occurrence and helps develop a second-year ENSO event by reinforcing the persistence of the PMM pattern.

We further use the Community Earth System Model, version 1 (CESM1), to study the low cloud–SST feedback. After confirming the nonlocal effect of the NEP low cloud–SST feedback in the model, we prescribe clouds from the control run to demonstrate the crucial mediating role of low cloud–SST feedback in modulating ENSO. These works shed light on the dynamics controlling the occurrence and duration of ENSO events, with implications for improving climate prediction.

Section 2 describes the data used in this study. Section 3 evaluates the summertime low cloud-SST feedback, in comparison with humidity gradient feedback and WES feedback over the subtropical NEP. Section 4 explores the role of NEP low cloud-SST feedback in ENSO evolution. Section 5 is a summary.

2. Data

We use a suite of observational and model simulations to examine the connection between low cloud–SST feedback and SST variability over the subtropical NEP. Our focus is on summer (June–August) when low cloud is prevalent over the subtropical NEP and the radiative effect is the strongest (Norris and Leovy 1994).

a. Observational datasets

Satellite data are used to investigate the cloud effect. Surface downward shortwave radiation flux is a useful parameter

to examine the impact of cloud on SST. We choose the monthly mean shortwave radiation flux provided by the International Satellite Cloud Climatology Project (ISCCP) on a $1^{\circ} \times 1^{\circ}$ grid during the years 1984–2018 (Zhang et al. 2004). The shortwave radiation flux data derive from the ISCCP-FH product. The use of surface shortwave radiation flux and that of cloud radiation effect yields similar results. This study adopts the former. The cloud fraction (CF) data from ISCCP-H product (1984–2018; Rossow and Schiffer 1999) are used to identify the low cloud region. ISCCP provides CF of different cloud types based on cloud-top pressure, including low-(1000–680 hPa), mid- (680–440 hPa), and high-level (440–10 hPa) categories. To improve the accuracy of our estimate of low cloud distribution, we combine the low- and midlevel CF and apply the random overlap assumption on the CF evaluation (Miyamoto et al. 2018).

For surface wind velocity, scalar surface wind speed, sea level pressure, and surface specific humidity, we use the ERA5 reanalysis provided by the European Centre for Medium-Range Weather Forecasts (ECMWF; Dee et al. 2011). ERA5 fields are on a $0.25^{\circ} \times 0.25^{\circ}$ grid. We use monthly Optimum Interpolation Sea Surface Temperature (OISST) on a $0.25^{\circ} \times$ 0.25° grid from the National Centers for Environmental Prediction to examine the relative wind direction to SST gradient. To investigate the responses of latent heat flux to SST variations, we also use surface latent heat flux from Objectively Analyzed Air-Sea Fluxes (OAFlux) on a 1° × 1° grid. The latent heat fluxes in OAFlux are calculated with COARE3.0 bulk algorithm using air-sea variables derived from the aforementioned satellite and reanalysis data. For clarity, statistical significance of related calculations is determined using a two-tailed t test at the 90% confidence level after correcting the degrees of freedom based on 1-yr lagged autocorrelation (Bretherton et al. 1999).

b. CESM1 simulations

To further examine the teleconnection of NEP low cloud-SST feedback and tropical SST, we use the preindustrial control simulation of CESM1 (Hurrell et al. 2013; Kay et al. 2015). CESM1 is a global coupled climate model composed of the atmosphere, ocean, land, and cryosphere components. The atmospheric component of CESM1 is the Community Atmosphere Model, version 5 (CAM5), which upgraded new advances including a new boundary layer, shallow convection, cloud macrophysics schemes, and fully interactive aerosols. The CESM1 control simulation is conducted with the f19_g16 grid of approximately 1° in the ocean model and approximately 2° horizontal resolution in the atmospheric model (CAM5), forced with preindustrial atmospheric greenhouse gas concentrations and interactive cloud with environment (Chen et al. 2021). A 200-yr-long simulation is performed, and the latest 150 years of the simulation are used because of the climate drift of the global mean temperature during the first 50 years due to the change in radiation coupling time (Chen et al. 2021). In this simulation, the instantaneous cloud properties are saved at every radiative time step that the radiation module is called (every 2 h). These variables include

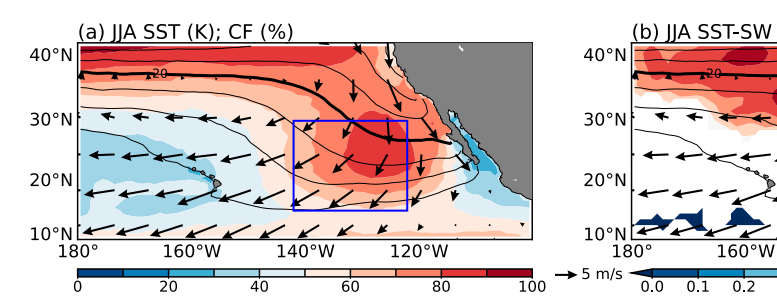


FIG. 1. JJA SST (contours, with 2-K interval), surface winds (vectors; m s⁻¹), and (a) cloud fraction (shading; %) and (b) correlation coefficients between JJA SSTAs and downward shortwave radiation flux anomalies (shading). Only the correlation coefficients that are statistically significant at 90% confidence level are plotted. The 20-K SST contours are thickened. The blue-outlined box (15°–30°N, 122°–142°W) indicates the low deck or cloudy area with large cloud fraction and high correlation coefficients between surface downward shortwave radiation and SST.

cloud fraction, snow cloud fraction, in-cloud liquid/ice/snow water path, size distribution parameters, and effective diameter for ice and snow.

We also examine a 150-yr-long cloud-locking experiment, where the cloud properties saved from the control run are used in the radiation module of CAM5 every 2 h to prevent the interaction between clouds and their surroundings (Chen et al. 2021). The cloud-locking experiment prescribes the specific year of clouds randomly from the last 30 years of the control run. The results are not sensitive to the choice of year for which cloud is prescribed. The cloud-locking experiment disables the cloud–ocean coupling globally. The mean climate is very similar between the control and cloud-locking runs because of similar cloud climatology.

3. Quantifying feedbacks of surface heat flux

a. Low cloud-SST feedback

Figure 1a shows the climatological mean low cloud fraction during summer over the subtropical NEP. Low clouds are frequently observed over the cold SST off the coast of Baja California, with the maximum cloud fraction of ~80% (Fig. 1a). The prevailing northerly trade winds on the eastern flank of the subtropical high blow from the north over the warm ocean, promoting the turbulent heat flux from sea surface. Descending motions cause strong capping inversions (Klein and Hartmann 1993; Norris and Leovy 1994). All these conditions contribute to the formation of low clouds.

Low clouds are closely coupled with the underlying SST through the modification of boundary layer processes. High correlations between surface downward shortwave radiation and SST are found over the low cloud region, supporting the positive radiative cloud feedback (Fig. 1b). We select the region of 15°–30°N, 122°–142°W with high correlation between SST and cloud fraction for our study (referred to herein as the NEP low cloud region). The distributions of low cloud fraction and the correlation with local SST are similar to those of Norris and Leovy (1994) based on ship reports.

b. Ocean mixed layer heat budget

The ocean mixed layer heat budget can be written as

$$C\frac{\partial T}{\partial t} = D_o + Q_{\text{net}},\tag{1}$$

120°W

where T is SST, C is the heat capacity of the mixed layer, and D_o is the ocean heat transport effect including the horizontal advection and upwelling. Surface flux $Q_{\rm net}$ (positive downward) includes four components $Q_{\rm net} = Q_S - Q_L - Q_E - Q_H$: solar radiation flux, net longwave radiation, latent heat flux, and sensible heat flux, respectively. In general, variability in net longwave radiation is much smaller than the shortwave variability at the surface. In the subtropical NEP, the Q_H and D_o are small (Xie et al. 2010). As a result, the low cloud shortwave radiative effect and the evaporative effect control the SST variability.

0.4 0.5

In the bulk formula, latent heat flux can be determined by the sea-air specific humidity gradient and surface wind speed. To separate the responses of dynamic (wind speed) and thermodynamic (humidity gradient) components to SSTAs, we decompose the latent heat flux by the linearization method. The surface upward latent heat flux can be described as follows:

$$Q_E = \rho_a L C_E W(q_s - q_a) = \rho_a L C_E (\overline{W} + W') \Delta(\overline{q} + q'), \quad (2)$$

where C_E is the turbulent moisture exchange coefficient, L is the latent heat of evaporation, ρ_a is the surface air density, W is the wind speed at 10 m above the surface, q_s is the saturated specific humidity at the surface calculated by SST and the Clausius–Clapeyron equation for saturation water vapor pressure, $q_a = \mathrm{RH}q_s(T_a)$ is air specific humidity at 2 m, T_a is air temperature at 2 m, and RH is relative humidity. Surface evaporation increases with wind speed and specific humidity gradient. The overbar represents the seasonal average, and the prime indicates the seasonal anomaly. We approximate the air–sea humidity gradient by a linear function of SST, $\Delta q' = \beta T'$. The linearized latent heat flux Eq. (1) becomes

$$Q_E' = \rho_a L C_E \overline{W} \Delta \overline{q} \left(\frac{W'}{\overline{W}} + \frac{\Delta q'}{\overline{\Delta q}} \right) = aW' + b_E T', \quad (3)$$

where $a=\overline{Q}_E/\overline{W}$ and $b_E=\alpha\overline{Q}_E$, with $\alpha=(1/\Delta\overline{q})(d\Delta\overline{q}/dT)$; $\Delta\overline{q}$ can also be written as $\Delta q=q_s(T_s)-\mathrm{RH}q_s(T_a)$. Here, α is

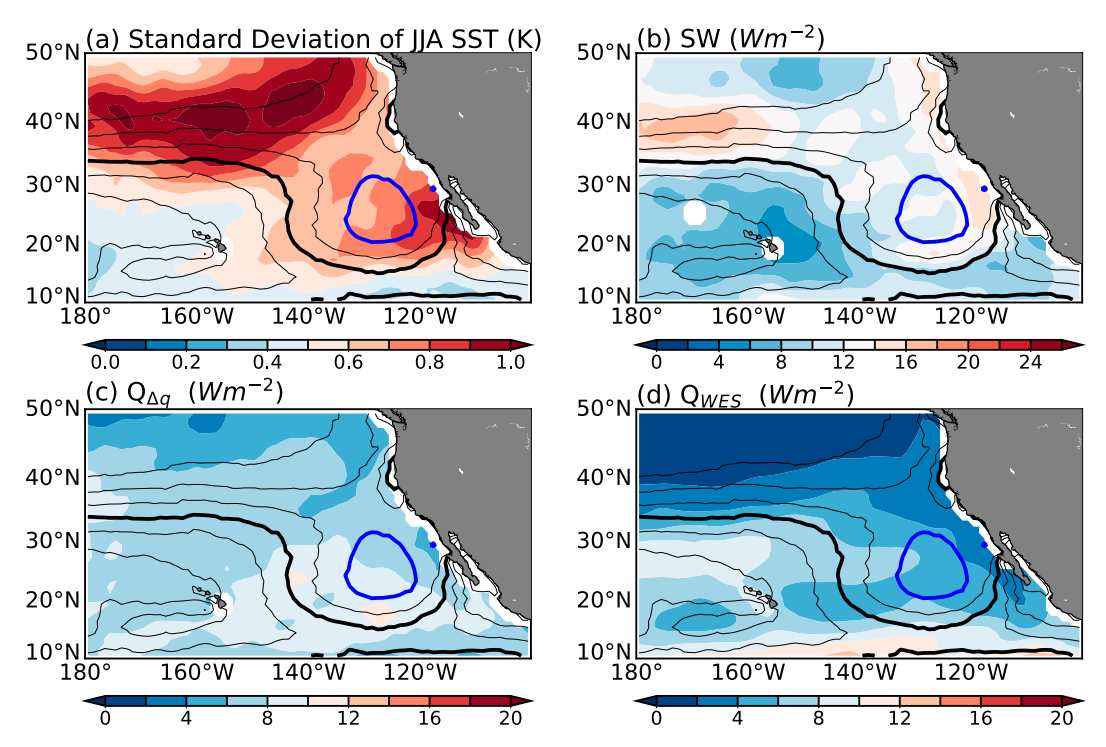


FIG. 2. JJA cloud fraction (contours, with 10% interval) and standard deviations for (a) SST (shading; K), (b) surface downward shortwave radiation flux (shading; W m⁻²), and latent heat flux arising from (c) humidity gradient (shading; W m⁻²) and (d) wind speed (shading; W m⁻²). The 50% and 80% cloud fraction levels are indicated by the thick black and blue contours, respectively. Note that (c) and (d) share the color bar with (b).

spatially varying and can be attained using seasonal averaged humidity gradient and linear regression of humidity gradient seasonal anomalies onto SST seasonal anomalies. Previous studies simplified α as a constant of 0.06 K⁻¹ (Xie et al. 2010) by assuming $T_s = T_a$ and RH = 80% because the sea-air temperature difference is small (~1°C) and RH ~ 80% over the open ocean with weak temperature advection. However, the real α values are not identical to the typical value over the subtropical NEP and even can reach nearly 3 times the typical value over the coastal area and central Pacific (not shown). In these regions, the T_s minus T_a difference is often larger temperature difference than 1°C and have relatively low regression coefficients (not shown). It is because the T_a and RH are mainly affected by the strong cold advection in the atmospheric boundary layer. Because the assumption is not totally practicable for the subtropical NEP, we use the realistic α but not the typical value in the following analysis.

Equation (3) suggests that the variations in latent heat flux can be divided into a thermodynamic component $b_E T'$ due to the sea–air humidity gradient anomalies and a dynamic component aW' driven by the wind speed anomalies. An increase in the sea–air humidity gradient due to a positive SST anomaly can increase evaporation and in turn damps the warm SST anomaly. We call this negative feedback evaporative damping. Likewise, an increase in surface wind speed increases evaporation, resulting in negative SSTAs, known as the WES feedback (Xie and Philander 1994; Xie 1999).

The linearized surface solar radiation can be cast as

$$Q_s' = b_c T', \tag{4}$$

where b_c is the cloud radiative effect. From Eqs. (3) and (4), the SST equation over the subtropical NEP is approximated as

$$C\frac{\partial T'}{\partial t} = Q'_s - Q'_E = -aW' + (b_c - b_E)T'.$$
 (5)

c. Comparison of three feedbacks

The decomposition of latent heat flux allows us to compare the evaporative damping and WES feedback with low cloud—SST feedback and identify which process primarily controls the local SST variability over the NEP low cloud region. Figure 2 shows the standard deviation (STD) of summer SST, surface downward solar radiation flux, and the surface heat flux due to evaporative damping and WES feedback. Over the cloudy region with cloud fraction greater than 50%, SST and solar radiation flux both have a large interannual variability, especially over the ocean north of 30°N, off the coast of Baja California (Figs. 2a,b). The STDs of SST and solar radiation flux are above 0.6 K and 10 W m⁻², respectively, over the NEP region where cloud fraction is greater than 50% (Figs. 2a,b). The STDs of the heat flux arising from evaporative damping and WES feedback are smaller than 10 W m⁻² (Figs. 2c,d).

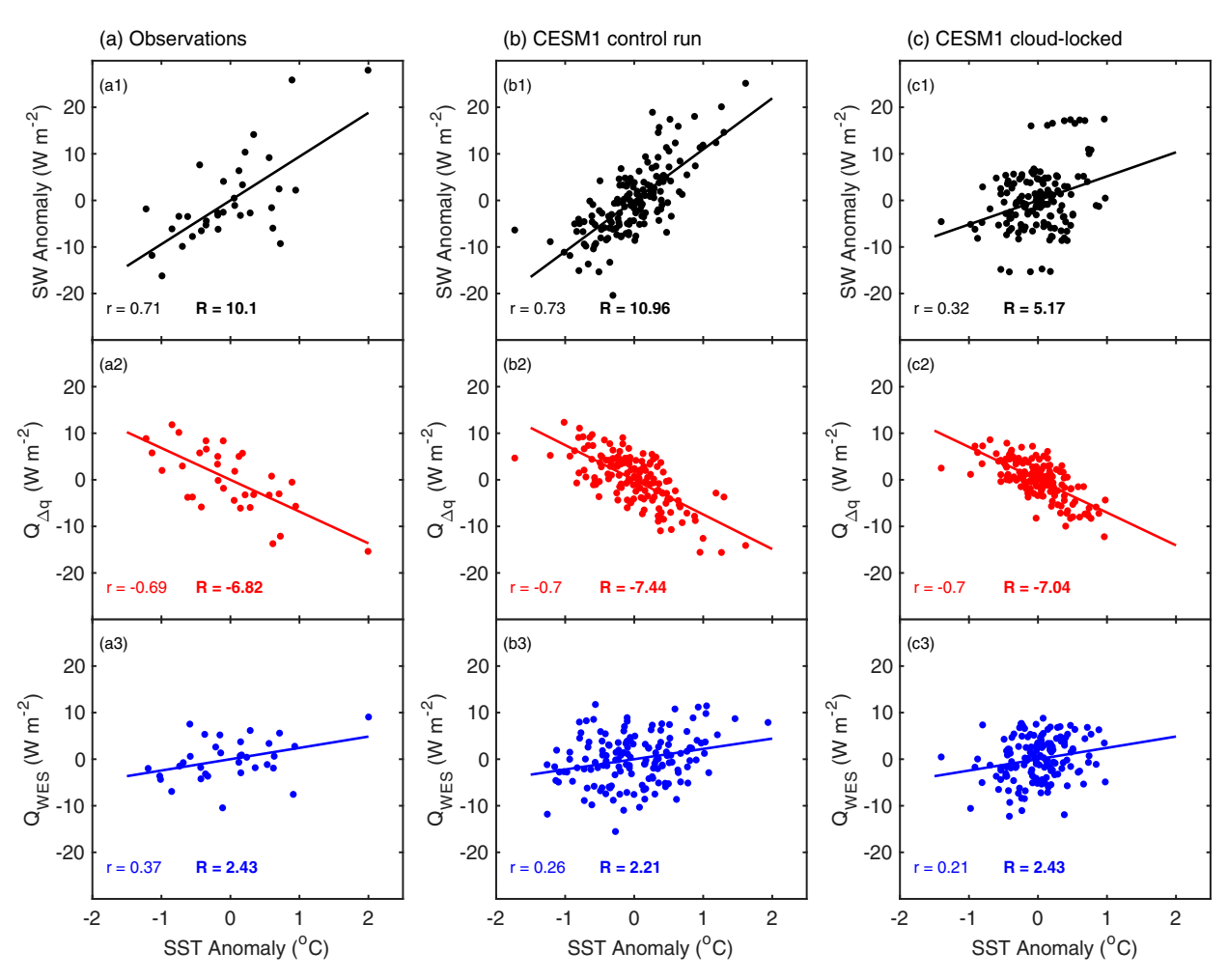


FIG. 3. Scatterplots of JJA SSTAs and (a1),(b1),(c1) surface downward shortwave radiation flux anomalies (black dots) and latent heat flux anomalies induced by (a2),(b2),(c2) humidity gradient (red dots) and (a3),(b3),(c3) wind speed (blue dots) based on the (a) observed data, (b) CESM1 control run, and (c) CESM1 cloud-locking experiment. All of the anomalies are averaged over the blue-outlined box in Fig. 1b. Here, *r* indicates the correlation coefficient, and *R* is the regression coefficient.

Also, the STD of the WES effect is much smaller than the evaporative damping effect. However, the STD of the WES feedback is strong and comparable to the STDs of the low cloud–SST and evaporative damping during spring (not shown). The STD analysis suggests that the low cloud–SST feedback is the largest variable among the three feedback processes over the NEP low cloud region, where the SST variability is high.

To further quantify the three feedback processes, we make the scatterplots of summertime regionally averaged SSTAs and surface downward heat flux anomalies due to the three feedback processes over the NEP low cloud region (Fig. 3). Low cloud–SST feedback has the highest correlation r = 0.74 and regression coefficient R = 10.79 W m⁻² K⁻¹among the three feedbacks (Fig. 3a). The evaporative damping is of secondary importance with r = -0.69 and reaches R = -6.82 W m⁻² K⁻¹ (Fig. 3b). The WES effect is the weakest over the NEP low cloud region during summer, inducing the smallest variation of surface downward heat flux (R = 2.43 W m⁻² K⁻¹; positive downward) among the three feedback processes (Fig. 3c). All

the above results clarify that, over the NEP low cloud region, the low cloud–SST feedback is the most important process for the local SST variability in summer.

Lagged correlation is used to identify the stochastic forcing and ocean response (Frankignoul 1985). Figure 4 shows the lagged correlations of surface downward solar radiation flux, latent heat flux due to humidity gradient, and wind speed with averaged SSTAs over the NEP low cloud region during June-August (JJA). The correlation with the WES effect is highly asymmetric about July, peaking in April-June, decreasing sharply in JJA (0.6 in June vs 0.3 in August) and becoming insignificant afterward (Fig. 4). The JJA SSTA correlation remains as high as 0.4 with the WES effect in antecedent February. This suggests a stochastic wind forcing in boreal spring but weak feedback from the ocean to the wind. The correlation with solar radiation and humidity gradient effect is consistent high (0.4-0.7) from March through December and largely symmetric about July. The strong low cloud-SST feedback contributes to the long persistence of SSTAs. JJA SSTAs are correlated at r = 0.7

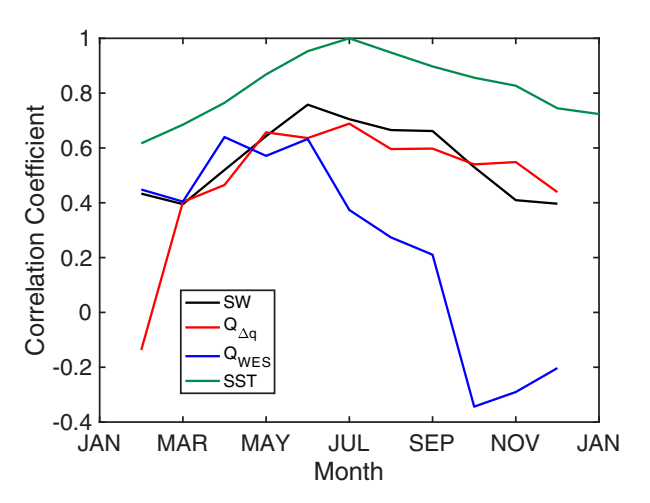


FIG. 4. Lagged correlation coefficients of 3-month averaged surface downward shortwave radiation flux (black line), latent heat flux due to the sea-air humidity gradient (red line), and scalar wind speed (blue line) with JJA SSTAs. All variables are averaged over the blue-outlined box in Fig. 1b. The correlation coefficients for latent heat flux anomalies induced by humidity gradient are plotted in reversed sign (red) for easy comparison. The autocorrelation for SST is in green.

with those in following December (Fig. 4). The air-sea humidity gradient is a damping effect on SSTA.

4. Remote impact on ENSO

a. Observational results

The local low cloud–SST feedback over the subtropical NEP affects large-scale SST variability over the North Pacific. Figure 5a shows the regression maps of JJA SSTAs, surface solar radiation flux and surface wind onto the time series of JJA SSTAs averaged over NEP low cloud region. It is evident that the NEP SSTAs are part of a large-scale SST pattern that resembles the PMM. The warm SSTAs over the NEP extend southwestward into the tropics, associated with a large-scale

cyclonic circulation and anomalous southwesterlies that contribute to the SST warming by weakening surface wind and evaporation (Fig. 5a). The high correlation between anomalies in SST and solar radiation flux over the subtropical NEP indicates strong positive feedback between low clouds and SST (Fig. 5a). Besides the solar radiation effect from low cloud, the reduced low clouds also weakened longwave radiative cooling at the cloud top, which can reinforce anomalous surface cyclonic winds (Nigam 1997; Rädel et al. 2016; Miyamoto et al. 2021, 2022).

A closer inspection shows that the strongest low cloud-SST feedback does not coincide with the center of the cloud deck (80% cloud fraction marked by the blue contour) but is displaced to the south where the gradients in the mean low cloud amount and SST are largest (Fig. 5a; Norris and Leovy 1994). Over the summertime subtropical NEP, the low cloud-SST feedback is also affected by the cold advection associated with the prevailing northeasterly winds. The southerly wind anomalies weaken the background northeasterly winds and cause reduced cold advection, reducing cloud cover through the weakened surface turbulent flux. The temperature advection anomalies reach maximum on the south flank of the low cloud deck, as a result of the coupled SST-wind anomaly pattern (Fig. 5b). The large temperature advection anomalies affect the low cloud-SST feedback and cause the phase difference between the low cloud-SST feedback and the mean cloud deck (Fig. 5a).

The regression pattern in Fig. 5a suggests that the local low cloud–SST feedback can affect the climate mode over the North Pacific by amplifying the SSTAs over the low cloud region and this warm signal extends southwestward into the deep tropics. To investigate the impact of NEP low cloud–SST feedback on the tropical SST variability, we regress anomalous SST and surface wind onto the time series of JJA SSTAs averaged over the NEP low cloud region (Fig. 6). We denote the year when the regionally averaged SST index is extracted as year 0 and divide a year into four seasons: spring is from March to May (MAM), summer is from June to August (JJA), autumn is from September to November (SON), and

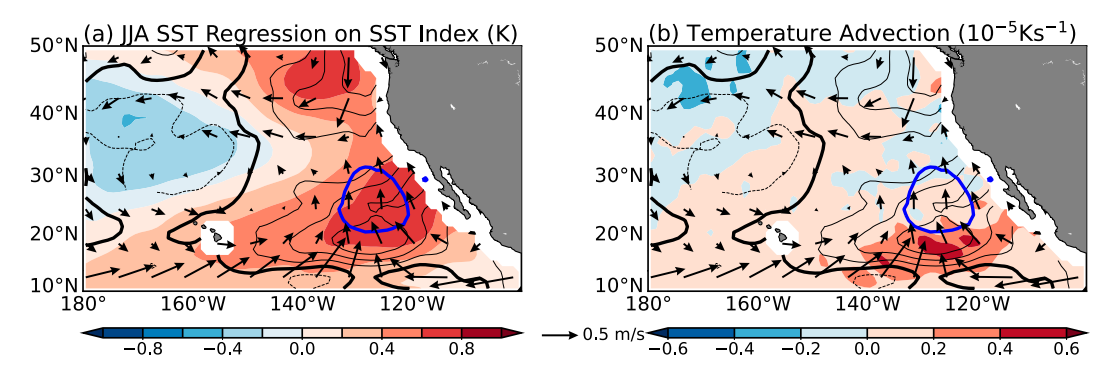


FIG. 5. Regression coefficients of JJA anomalous surface downward shortwave radiation flux (contours, with 2.5 W m $^{-2}$ K $^{-1}$ interval), wind (vectors; m s $^{-1}$ K $^{-1}$), (a) SST (shading; K K $^{-1}$) and (b) temperature advection (shading; 10^{-5} K s $^{-1}$ K $^{-1}$) onto the time series of JJA SSTAs averaged over the blue-outlined box in Fig. 1b. The thickened blue contours represent the 80% cloud fraction, and the thickened black contours indicate the level of zero shortwave radiation flux.

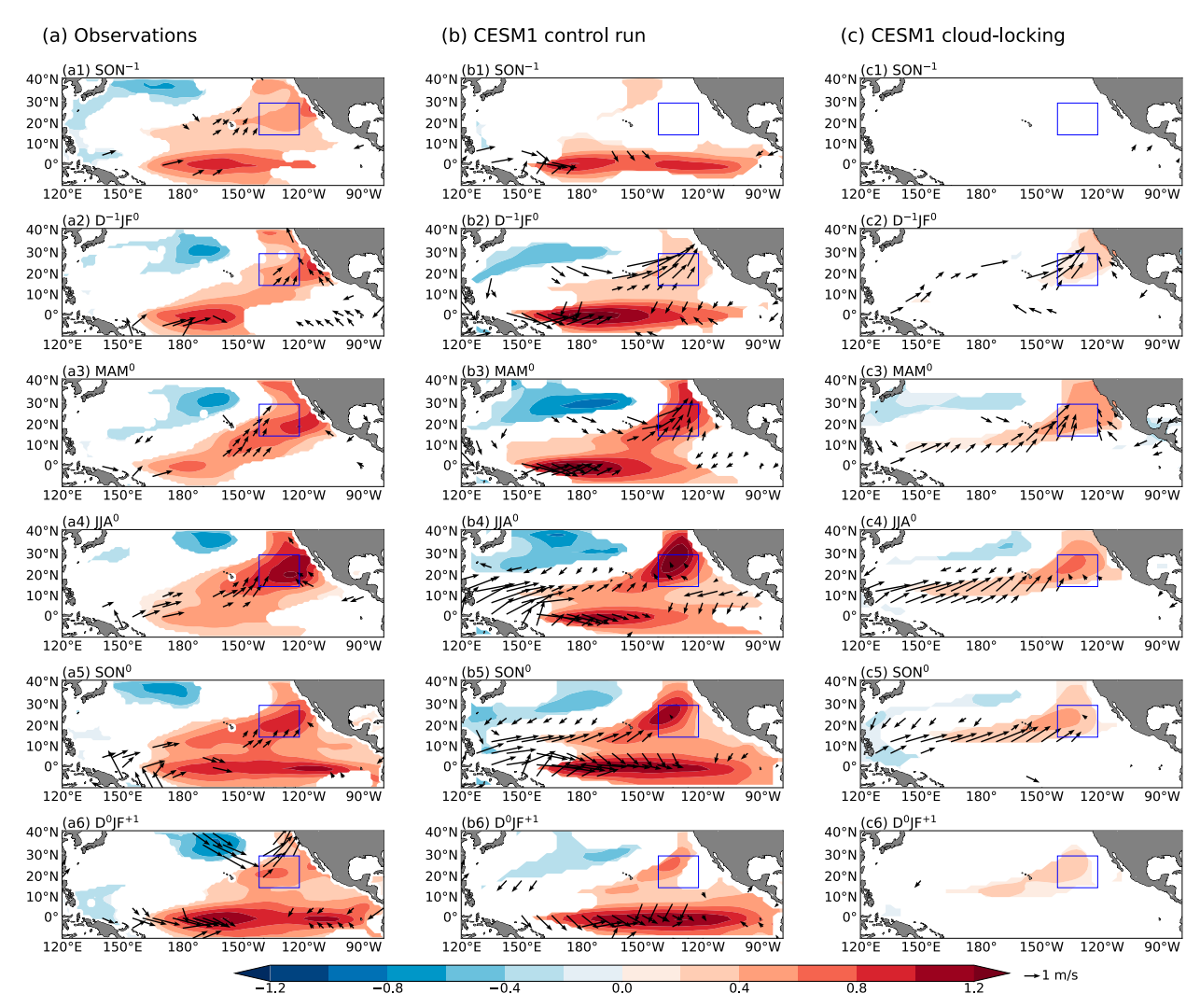


FIG. 6. Regression coefficients of seasonal SSTAs (shading; $K K^{-1}$) and wind anomalies (vectors; $m s^{-1} K^{-1}$) onto the time series of JJA SSTAs averaged over the blue-outlined box based on the (a) observed data, (b) CESM1 control run, and (c) CESM1 cloud-locking experiment. Year 0 denotes the year when the regionally averaged SST index is extracted. Only the regression coefficients that are statistically significant at 90% confidence level are plotted.

winter is from December to next February (DJF). These regressions span two years from SON⁻¹ to D⁰JF¹, where superscript numbers indicate the previous (-1), present (0), and following (1) year. To focus on the interannual variability of these variables, we remove the low-frequency signals by applying a 10-yr high-pass Lanczos filter on every time series.

The SSTAs over the subtropical NEP develop during D⁻¹JF⁰, in response to anomalous southerlies (Fig. 6a2). The southwesterly wind anomalies weaken the background northeasterly trade winds, reducing evaporative cooling at the surface to warm the ocean. These warm anomalies over NEP grow in MAM⁰, peak in JJA⁰, and persist throughout the following SON⁰ and D⁰JF⁺¹ (Figs. 6a3–a6). From the subtropical NEP, the coupled warm SSTAs and southwesterly wind anomalies propagate southwestward through the WES feedback into the deep tropics (Figs. 6a3–a6). Here the NEP low

cloud deck serves as the "source" region where SST variability is amplified by the strong cloud-SST feedback.

Upon arriving at the equator, the westerly wind anomalies on the equator are enhanced, which weakens the background easterly trade winds and amplifies the equatorial warm signal through ocean dynamical feedbacks that amplify warm SSTAs across the basin (Amaya et al. 2019). As a result, El Niño-like SSTAs begin to grow during SON⁰ in the eastern equatorial Pacific (Fig. 6a5). On the equator, the eastward displacement of the warm SSTAs relative to the westerly wind anomalies suggests the importance of ocean dynamics. From SON⁰ to D⁰JF¹, the equatorial SST and wind anomalies strengthen through Bjerknes feedback, characteristic of El Niño growth (Figs. 6a5–a6). While they support the PMM effect on ENSO in the literature, our results show that the NEP low cloud–SST feedback is key to the connection by amplifying the PMM.

Coherent warm SST and westerly wind anomalies over the west equatorial Pacific in the antecedent winter D⁻¹JF⁰ suggest a relationship between summertime low cloud-SST feedback over the subtropical NEP and 2-yr ENSO event (Fig. 6a2). Following an antecedent El Niño, equatorial SST and wind anomalies weaken in MAM⁰ and JJA⁰ (Figs. 6a3,a4), only to be reintensified by the remote effect of the summertime low cloud-SST feedback on the subtropical NEP, resulting in a second-year El Niño event in the subsequent winter (Figs. 6a5,a6). Thus, the 2-yr El Niño event is more likely to occur when there are warm anomalies over the subtropical NEP in summer following El Niño in the previous year and the 2-yr La Niña event is more likely to occur when there are cold anomalies over the subtropical NEP in summer following La Niña in the previous year. The nonlocal effect of NEP low cloud-SST feedback prevents the equatorial warm anomalies from dissipating after the first-year El Niño and reinforces the warm signal, leading to a 2-yr El Niño event. The nonlocal effect of NEP low cloud-SST feedback also prevents the equatorial cold anomalies from dissipating after the first-year La Niña and reinforces the cold signal, leading to a 2-yr La Niña event.

b. Model results

We use the CESM1 simulations to examine the relationship between the low cloud-SST feedback and ENSO. The CESM1 can reproduce the SST variability and the feedback processes over the subtropical northeast Pacific. In the CESM1 control run, SST have a large interannual variability over the NEP cloudy region. The STD of JJA SST averaged over the NEP low cloud region is 0.69 K, close to the 0.72 K in the observations. The correlation and regression coefficients of the low cloud-SST feedback (r = 0.73; $R = 10.96 \text{ W m}^{-2} \text{ K}^{-1}$) are close to the observed results over the NEP low cloud region (Figs. 3a1,b1). The evaporative damping effect in the CESM1 model ($R = -7.44 \text{ W m}^{-2} \text{ K}^{-1}$) is slightly stronger than that in the observations (Fig. 3b). The WES effect is well produced in the CESM1 control run ($R = 2.43 \text{ W m}^{-2} \text{ K}^{-1}$; Fig. 3c). When the cloud is noninteractive, the JJA SST STD over the NEP low cloud region is reduced by 25% (0.52 K), so are the correlation and regression coefficients between the SW and SST $(r = 0.32 \text{ and } R = 5.17 \text{ W m}^{-2} \text{ K}^{-1}; \text{ Figs. 3a1,b1}).$ The changes in evaporative damping and the WES effect are small and insignificant in the cloud-locking experiment (Fig. 3b). ENSO in CESM1 is well simulated, although the Niño-3.4 SST variance is overestimated (Hurrell et al. 2013; Zheng et al. 2018). The STDs of DJF Niño-4 SST in the observations, CESM1 control run, and cloud-locking experiment are 0.98, 1.04, and 0.95 K, respectively. The averaged DJF Niño-4 SSTAs during El Niño years in observations, CESM1 control run, and cloud-locking experiment are 1.42, 1.56, and 1.66 K, respectively. The averaged DJF Niño-4 SSTAs during La Niña years in observations, CESM1 control run, and cloud-locking experiment are -1.44, -1.7, and −1.56 K, respectively.

Figures 6b and 6c show the same lead-lag regression maps as Fig. 6a but for the model. The CESM1 simulation

successfully captures the evolution of the SSTAs and wind anomalies. The SST and wind patterns over the north and tropical Pacific show a similar evolution to the observed results through D⁻¹JF⁰ to D⁰JF⁺¹, but more coherent with a larger magnitude (Figs. 6a,b). There is a coherent anomalous cyclone over the North Pacific in D⁻¹JF⁰, which is not obvious in the observational results. The enhanced spatiotemporal coherence is possibly due to suppressed noise by using the 150-yr-long CESM1 simulation (Fig. 6a2,b2). After D⁻¹JF⁰, summertime low cloud feedback over the subtropical NEP amplifies the local warm SSTAs and promotes their southwestward propagation, promoting the equatorial warm SST and westerly wind anomalies and El Niño (Figs. 6b4-b6). The model results also exhibit a significant antecedent El Niño event, with a larger magnitude of warm SSTAs on the equator than that in the observed results (Figs. 6a2,b2). These warm anomalies and westerly wind anomalies weaken in MAM⁰ and persist in JJA⁰ due to the teleconnection effect of the NEP low cloud-SST feedback (Figs. 6b3,b4). Then the equatorial SST and wind anomalies amplify and cover the whole equator in SON⁰ and D⁰JF⁺¹, resulting in a secondyear El Niño (Figs. 6b5,b6). The model results support that the NEP low cloud-SST feedback contributes to the occurrence and duration of ENSO events.

The cloud-locking experiment further demonstrates the important effects of NEP low cloud–SST feedback on ENSO. When the low cloud–SST feedback is disabled, warm SSTAs still occur in D⁻¹JF⁰ under the anomalous southerly wind over the subtropical NEP and propagate southwestward because of WES feedback, but at a much-reduced magnitude relative to observations and the CESM1 control run (Figs. 6c2–c6). The warm SST and wind anomalies are limited north of 10°N and have no obvious effect on the equatorial SST and wind (Figs. 6c2–c6). This result shows that the NEP SSTAs cannot trigger ENSO events solely through WES feedback, suggesting the crucial role of low cloud–SST feedback in PMM modulation of ENSO.

To further reveal the effect of the NEP low cloud-SST feedback on ENSO development, we regress equatorial (5°S-5°N, 140°E-80°W) SST and surface wind anomalies against JJA⁰ SST over the NEP low cloud region (Fig. 7). Both the observations and CESM1 control run display a 2-yr El Niño event, with a larger magnitude in CESM1 than the observations (Figs. 7a,b). The equatorial warm SST and westerly wind anomalies peak in the western equatorial Pacific in November⁻¹ and February⁰ for observations and CESM1, respectively, indicative of the first-year El Niño (Figs. 7a,b). Then the equatorial warm SSTAs begin to weaken through June⁰ (Figs. 7a,b). During January⁰-June⁰, the warm SSTAs persist only in the western Pacific in observations but they cover the whole equatorial Pacific in the model (Figs. 7a,b). The warm SST and westerly wind anomalies begin to intensify after August⁰, as a result of the PMM that emanates from the NEP, energized by low cloud-SST feedback (Figs. 7a,b). When the low cloud-SST feedback is disabled, the correlation between the NEP and equatorial Pacific vanishes (Fig. 7c).

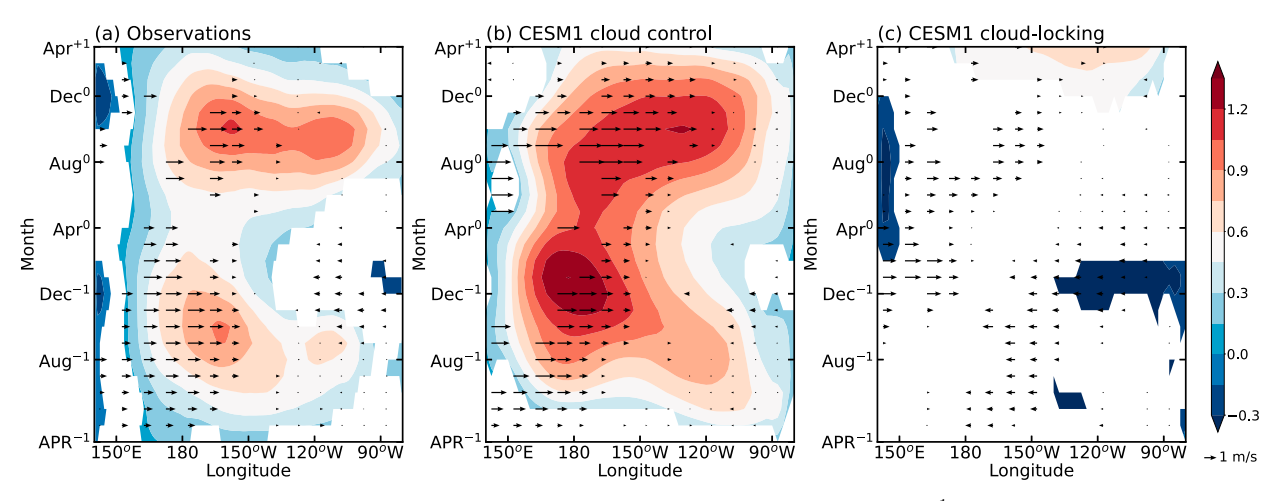


FIG. 7. Hovmöller diagrams of meridionally averaged ($5^{\circ}S-5^{\circ}N$, $140^{\circ}E-80^{\circ}W$) SST (shading; K K⁻¹) and surface zonal wind (vectors; m s⁻¹ K⁻¹) from Apr⁻¹ to Apr⁺¹ regressed onto the time series of JJA⁰ SSTAs averaged over the blue-outlined box in Fig. 1 based on the (a) observed data, (b) CESM1 control run, and (c) CESM1 cloud-locking experiment. Only the regression coefficients that are statistically significant at 90% confidence level are plotted.

We have also examined a 1500-yr-long CESM1 control run at enhanced atmospheric model resolution (\sim 1° \times 1°) to increase the number of ENSO events. The results from the high-resolution simulation are similar to those from our 150-yr-long control simulation, except that the first-year ENSO event is of larger equatorial SSTAs.

Figure 8 shows the scatterplot of NEP SSTAs against Niño-4 (5S-5°N, 160°E-150°W) SSTAs in the following winter. We focus on years preceded by an El Niño (red dots) or La Niña (blue dots) event selected from the 1500-yr CESM1 control run. When summer SSTA over the low cloud region is positive (negative), the Niño-4 SST anomalies tend to be positive (negative) in the following winter. The significant positive correlation between the NEP and Niño-4 SST anomalies (r = 0.36)

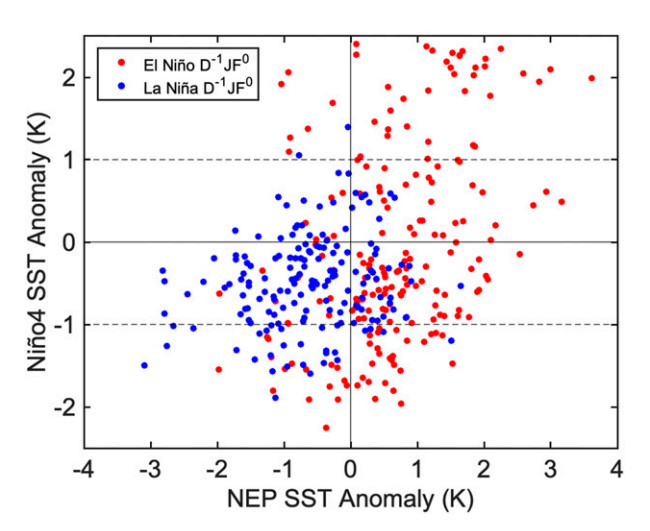


FIG. 8. Evolution of El Niño (DJF Niño-4 > 1 K; red dots) and La Niña (DJF Niño-4 < -1 K; blue dots) events in the 1500-yrlong CESM1 control run, as shown in a scatterplot for NEP SSTA in the subsequent JJA and Niño-4 SSTA in the subsequent DJF.

for all the selected events indicates a linkage between the subtropics and tropics in the ENSO evolution (Fig. 8). One-fourth of the El Niño events evolve into 2-yr events, and significant positive SSTAs over the NEP stratus deck region that exceed 1 STD play an intermediate or bridge role in one-half of these 2-yr events. This result supports that the 2-yr El Niño event is more likely to occur when the summer SSTAs are positive over the subtropical NEP following an antecedent El Niño event. Conversely, one-fourth of the La Niña events evolve into 2-yr events, and significant negative SSTAs over the NEP stratus deck region that exceed 1 STD play an intermediate or bridge role in one-half of these 2-yr events. This result supports that the 2-yr La Niña event is more likely to occur when the summer SSTAs are negative over the subtropical NEP following an antecedent La Niña event.

In observations, there seems a preference for 2-yr La Niña events while this asymmetry between El Niño and La Niña is not so obvious in the 1500-yr-long CESM1 run (Fig. 8). Fang and Yu (2020) suggest that an antecedent La Niña can trigger a negative PMM event through an anomalous anticyclone and subsidence over the NEP, in favor of another La Niña event in the following year. Our observational and model analyses (Figs. 1–7) highlight the important role of summertime low cloud–SST feedback over the NEP in energizing the PMM, which goes on to force multiyear ENSO events. The PMM modulation mechanism can cause asymmetry between El Niño and La Niña events (Dommenget et al. 2013; Timmermann et al. 2018; Yu and Fang 2018). In CESM1, 22% of El Niño events evolves into La Niña (red dots with Niño-4 < -1 in Fig. 8) whereas La Niña almost never evolves into El Niño.

5. Summary

Low clouds are prevalent over the NEP during summer and interact with SST through a positive radiative feedback. We use long-term observations to determine the role of low cloud–SST feedback over the summertime subtropical NEP

in local SST and ENSO variability. Our results reveal that low cloud–SST feedback is dominant for local SST variations over the subtropical NEP and contributes to the ENSO occurrence and evolution. The model simulations confirm the role of low cloud–SST feedback over the NEP.

Surface latent heat flux is another important process for the SST variations over the subtropical North Pacific. Quantitative analysis shows that the low cloud-SST feedback is strongest $(R = 10.1 \text{ W m}^{-2} \text{ K}^{-1})$ when compared with the evaporative damping ($R = -6.82 \text{ W m}^{-2} \text{ K}^{-1}$) and WES effect $(R = 2.43 \text{ W m}^{-2} \text{ K}^{-1})$ over the NEP low cloud region during summer. The lagged correlations with JJA SST indicate distinct roles of these feedbacks. The low cloud and humidity gradient are strong feedback on SSTAs (positive and negative, respectively). In fact, the low cloud-SST feedback exceeds the negative evaporative damping, suggesting that the summer NEP might be locally unstable thermodynamically. Over the NEP, the WES feedback is weak in summer and represents stochastic wind forcing as indicated by lagged cross-correlation with SST. These results identify low cloud-SST feedback as the dominant mechanism amplifying SST variability over the summer subtropical NEP.

Low cloud-SST feedback is often considered local. This might indeed be the case physically but SSTAs induce largescale wind response and the resultant WES feedback causes the coupled SST-wind anomalies to propagate southwestward. Our analysis of long-term observations shows that the PMM pattern, forced by anomalous wind in boreal winter, is energized by the low cloud-SST feedback in summer over the NEP low cloud deck. Because of the joint cloud-WES feedback, positive SSTAs and anomalous westerly wind propagate from the NEP southwestward, causing El Niño upon arriving at the equator and, conversely, negative SSTAs and anomalous easterly wind propagate from the NEP southwestward, causing La Niña upon arriving at the equator. NEP SST variability seems to mediate 2-yr ENSO events. A 2-yr El Niño event tends to be associated with positive SSTAs and a 2-yr La Niña event tends to be associated with negative SSTAs over the NEP cloud deck during the intermediate summer, consistent with model prediction experiments (Wu et al. 2021).

CESM1 is used to examine the role of low cloud–SST feedback in ENSO variability. The CESM1 control run successfully captures the observed evolution of SST and wind anomalies as in the observations. When the low cloud–SST feedback is disabled in the cloud-locking experiment, the NEP SSTAs extend southwestward but the propagation is limited to the north of 10°N without an obvious effect on the deep tropics. This suggests that low cloud–SST feedback is an important bridge for extratropical signals to propagate into the equatorial Pacific and that summer NEP SST conditions are a source of ENSO predictability, especially with regard to whether an ENSO event will reintensify and evolve into a second-year event (DiNezio et al. 2017; Wu et al. 2021).

PMM-like patterns emerge in climate models in response to high-latitude energy perturbations from single hemisphere (Hwang et al. 2017; Kang et al. 2021; Hsiao et al. 2022; Luongo et al. 2022). Joint low cloud–WES feedback produces

a tongue-like structure in SST that emanates from the low cloud deck in the eastern subtropical ocean and extends equatorward and westward, much like what we describe here based on observations. Subtropical low cloud radiative feedback has been shown to control the magnitude of the SST pattern. While CESM1 has been identified as extremely strong in cloud feedback within a multimodel ensemble (Kim et al. 2022), Fig. 3 shows that the model is very realistic in comparison with observations, highlighting the importance of observational constraints.

Acknowledgments. Authors Yang and Liu are supported by the National Key Research and Development Program of China (2018YFA0605700), the Natural Science Foundation of China (41875012), and Natural Science Foundation of Shandong Province (ZR2019ZD12); author Xie is supported by the National Science Foundation (AGS 2105654); and author Hwang is supported by the Ministry of Science and Technology in Taiwan MOST (111-2628-M-002-003). We acknowledge the ECMWF (ERA5), the National Centers for Environmental Prediction (SST), the Satellite Cloud Climatology Project (ISCCP), and the National Center for Atmospheric Research (CESM1) for providing data.

Data availability statement. The 1500-yr CESM1 control simulation is available online (https://www.cesm.ucar.edu). The output from the 150-yr control and cloud-locking runs is available upon request. The ERA5 data are available at https://www.ccmwf.int/en/forecasts/datasets/reanalysis-datasets/era5; the OISST data are available at https://www.ncei.noaa.gov/products/optimum-interpolation-sst; and the OAFlux data are available at https://oaflux.whoi.edu.

REFERENCES

Amaya, D. J., Y. Kosaka, W. Zhou, Y. Zhang, S.-P. Xie, and A. J. Miller, 2019: The North Pacific pacemaker effect on historical ENSO and its mechanisms. *J. Climate*, 32, 7643–7661, https://doi.org/10.1175/JCLI-D-19-0040.1.

Bellomo, K., A. Clement, T. Mauritsen, G. Rädel, and B. Stevens, 2014: Simulating the role of subtropical stratocumulus clouds in driving Pacific climate variability. *J. Climate*, 27, 5119–5131, https://doi.org/10.1175/JCLI-D-13-00548.1.

—, A. C. Clement, and T. Mauritsen, G. R\u00e4del, and B. Stevens, 2015: The influence of cloud feedbacks on equatorial Atlantic variability. J. Climate, 28, 2725–2744, https://doi.org/10.1175/ JCLI-D-14-00495.1.

—, —, L. N. Murphy, L. M. Polvani, and M. A. Cane, 2016: New observational evidence for a positive cloud feedback that amplifies the Atlantic multidecadal oscillation. *Geophys. Res. Lett.*, 43, 9852–9859, https://doi.org/10. 1002/2016GL069961.

Bretherton, C. S., M. Widmann, V. P. Dymnikov, J. M. Wallace, and I. Bladé, 1999: The effective number of spatial degrees of freedom of a time-varying field. *J. Climate*, **12**, 1990–2009, https://doi.org/10.1175/1520-0442(1999)012<1990:TENOSD>2. 0.CO:2.

Brown, P. T., M. S. Lozier, R. Zhang, and W. Li, 2016: The necessity of cloud feedback for a basin-scale Atlantic multidecadal

- oscillation. *Geophys. Res. Lett.*, **43**, 3955–3963, https://doi.org/10.1002/2016GL068303.
- Chen, Y. J., Y. T. Hwang, and P. Ceppi, 2021: The impacts of cloud-radiative changes on poleward atmospheric and oceanic energy transport in a warmer climate. *J. Climate*, 34, 7857–7874, https://doi.org/10.1175/JCLI-D-20-0949.1.
- Chiang, J. C. H., and D. J. Vimont, 2004: Analogous Pacific and Atlantic meridional modes of tropical atmosphere–ocean variability. J. Climate, 17, 4143–4158, https://doi.org/10.1175/ JCLI4953.1.
- Clement, A. C., R. Burgman, and J. R. Norris, 2009: Observational and model evidence for positive low-level cloud feedback. *Science*, 325, 460–464, https://doi.org/10.1126/science. 1171255.
- Dee, D. P., and Coauthors, 2011: The ERA-Interim reanalysis: Configuration and performance of the data assimilation system. *Quart. J. Roy. Meteor. Soc.*, **137**, 553–597, https://doi.org/10.1002/qj.828.
- DiNezio, P. N., C. Deser, Y. Okumura, and A. Karspeck, 2017: Predictability of 2-year La Niña events in a coupled general circulation model. *Climate Dyn.*, 49, 4237–4261, https://doi. org/10.1007/s00382-017-3575-3.
- Dommenget, D., T. Bayr, and C. Frauen, 2013: Analysis of the non-linearity in the pattern and time evolution of El Niño southern oscillation. *Climate Dyn.*, **40**, 2825–2847, https://doi.org/10.1007/s00382-012-1475-0.
- Evan, A. T., R. J. Allen, R. Bennartz, and D. J. Vimont, 2013: The modification of sea surface temperature anomaly linear damping time scales by stratocumulus clouds. *J. Climate*, **26**, 3619–3630, https://doi.org/10.1175/JCLI-D-12-00370.1.
- Fairall, C. W., E. F. Bradley, D. P. Rogers, J. B. Edson, and G. S. Young, 1996: Bulk parameterization of air–sea fluxes for Tropical Ocean–Global Atmosphere Coupled Ocean–Atmosphere Response Experiment. J. Geophys. Res., 101, 3747–3764, https://doi.org/10.1029/95JC03205.
- —, J. E. Hare, A. A. Grachev, and J. B. Edson, 2003: Bulk parameterization of air–sea fluxes: Updates and verification for the COARE algorithm. *J. Climate*, **16**, 571–591, https://doi.org/10.1175/1520-0442(2003)016<0571:BPOASF>2.0.CO;2.
- Fang, S. W., and J. Y. Yu, 2020: A control of ENSO transition complexity by tropical Pacific mean SSTs through tropicalsubtropical interaction. *Geophys. Res. Lett.*, 47, e2020GL087933, https://doi.org/10.1029/2020GL087933.
- Frankignoul, C., 1985: Sea surface temperature anomalies, planetary waves, and air–sea feedback in the middle latitudes. *Rev. Geophys.*, **23**, 357–390, https://doi.org/10.1029/RG023i004p00357.
- Horii, T., and K. Hanawa, 2004: A relationship between timing of El Niño onset and subsequent evolution. *Geophys. Res. Lett.*, **31**, L06304, https://doi.org/10.1029/2003GL019239.
- Hsiao, W.-T., Y.-T. Hwang, Y.-J. Chen, and S. M. Kang, 2022: The role of clouds in shaping tropical Pacific response pattern to extratropical thermal forcing. *Geophys. Res. Lett.*, 49, e2022GL098023, https://doi.org/10.1029/2022GL098023.
- Hurrell, J. W., and Coauthors, 2013: The Community Earth System Model: A framework for collaborative research. *Bull. Amer. Meteor. Soc.*, 94, 1339–1360, https://doi.org/10.1175/BAMS-D-12-00121.1.
- Hwang, Y.-T., S.-P. Xie, C. Deser, and S. M. Kang, 2017: Connecting tropical climate change with Southern Ocean heat uptake. *Geophys. Res. Lett.*, 44, 9449–9457, https://doi.org/10.1002/2017GL074972.

- Jong, B. T., M. Ting, R. Seager, and W. B. Anderson, 2020: ENSO teleconnections and impacts on U.S. summertime temperature during a multiyear La Niña life cycle. *J. Climate*, 33, 6009–6024, https://doi.org/10.1175/JCLI-D-19-0701.1.
- Kang, S. M., S.-P. Xie, C. Deser, and B. Xiang, 2021: Zonal mean and shift modes of historical climate response to evolving aerosol distribution. *Sci. Bull.*, 66, 2405–2411, https://doi.org/ 10.1016/j.scib.2021.07.013.
- Kay, J. E., and Coauthors, 2015: The Community Earth System Model (CESM) Large Ensemble project: A community resource for studying climate change in the presence of internal climate variability. *Bull. Amer. Meteor. Soc.*, 96, 1333–1349, https://doi.org/10.1175/BAMS-D-13-00255.1.
- Kim, H., S. M. Kang, J. E. Kay, and S.-P. Xie, 2022: Subtropical clouds key to Southern Ocean teleconnections to the tropical Pacific. *Proc. Natl. Acad. Sci. USA*, 119, e2200514119, https:// doi.org/10.1073/pnas.2200514119.
- Klein, S. A., and D. L. Hartmann, 1993: The seasonal cycle of low stratiform clouds. *J. Climate*, 6, 1587–1606, https://doi.org/10. 1175/1520-0442(1993)006<1587:TSCOLS>2.0.CO;2.
- —, —, and J. R. Norris, 1995: On the relationships among low-cloud structure, sea surface temperature, and atmospheric circulation in the summertime northeast Pacific. *J. Climate*, **8**, 1140–1155, https://doi.org/10.1175/1520-0442(1995) 008<1140:OTRALC>2.0.CO;2.
- Lee, S.-K., P. N. DiNezio, E.-S. Chung, S.-W. Yeh, A. T. Wittenberg, and C. Wang, 2014: Spring persistence, transition and resurgence of El Niño. *Geophys. Res. Lett.*, 41, 8578–8585, https://doi.org/10.1002/2014GL062484.
- Luongo, M. T., S.-P. Xie, and I. Eisenman, 2022: Buoyancy foreing dominates cross-equatorial ocean heat transport response to hemispheric cooling. *J. Climate*, 35, 3071–3090, https://doi. org/10.1175/JCLI-D-21-0950.1.
- Middlemas, E., A. Clement, and B. Medeiros, 2019: Contributions of atmospheric and oceanic feedbacks to subtropical northeastern sea surface temperature variability. *Climate Dyn.*, **53**, 6877–6890, https://doi.org/10.1007/s00382-019-04964-1.
- Miyamoto, A., H. Nakamura, and T. Miyasaka, 2018: Influence of the subtropical high and storm track on low-cloud fraction and its seasonality over the south Indian Ocean. *J. Climate*, **31**, 4017–4039, https://doi.org/10.1175/JCLI-D-17-0229.1.
- —, —, and Y. Kosaka, 2021: Radiative impacts of low-level clouds on the summertime subtropical high in the south Indian Ocean simulated in a coupled general circulation model. *J. Climate*, 34, 3991–4007, https://doi.org/10.1175/JCLI-D-20-0709.1.
- —, —, and —, 2022: Wintertime weakening of low-cloud impacts on the subtropical high in the south Indian Ocean. *J. Climate*, **35**, 323–334, https://doi.org/10.1175/JCLI-D-21-0178.1.
- Myers, T. A., C. R. Mechoso, and M. J. DeFlorio, 2017: Importance of positive cloud feedback for tropical Atlantic interhemispheric climate variability. *Climate Dyn.*, 51, 1707–1717, https://doi.org/10.1007/s00382-017-3978-1.
- —, G. V. Cesana, M. J. DeFlorio, and D. E. Waliser, 2018a: Cloud feedback key to marine heatwave off Baja California. *Geophys. Res. Lett.*, **45**, 4345–4352, https://doi.org/10.1029/2018GL078242.
- —, —, and J. M. DeFlorio, 2018b: Coupling between marine boundary layer clouds and summer-to-summer sea surface temperature variability over the North Atlantic and Pacific. *Climate Dyn.*, **50**, 955–969, https://doi.org/10.1007/s00382-017-3651-8.

- Nigam, S., 1997: The annual warm to cold phase transition in the eastern equatorial Pacific: Diagnosis of the role of stratus cloud-top cooling. *J. Climate*, **10**, 2447–2467, https://doi.org/10.1175/1520-0442(1997)010<2447:TAWTCP>2.0.CO;2.
- Norris, J. R., and C. B. Leovy, 1994: Interannual variability in stratiform cloudiness and sea surface temperature. *J. Climate*, 7, 1915–1925, https://doi.org/10.1175/1520-0442(1994)007<1915: IVISCA>2.0.CO;2.
- —, Y. Zhang, and J. M. Wallace, 1998: Role of low clouds in summertime atmosphere–ocean interactions over the North Pacific. *J. Climate*, 11, 2482–2490, https://doi.org/10.1175/1520-0442(1998)011<2482:ROLCIS>2.0.CO;2.
- Ohba, M., and H. Ueda, 2009: Role of nonlinear atmospheric response to SST on the asymmetric transition process of ENSO. J. Climate, 22, 177–192, https://doi.org/10.1175/ 2008JCLJ2334.1.
- Okumura, Y. M., 2019: ENSO diversity from an atmospheric perspective. *Curr. Climate Change Rep.*, **5**, 245–257, https://doi.org/10.1007/s40641-019-00138-7.
- —, and C. Deser, 2010: Asymmetry in the duration of El Niño and La Niña. *J. Climate*, 23, 5826–5843, https://doi.org/10.1175/2010JCLI3592.1.
- Rädel, G., T. Mauritsen, B. Stevens, D. Dommenget, D. Matei, K. Bellomo, and A. Clement, 2016: Amplification of El Niño by cloud longwave coupling to atmospheric circulation. *Nat. Geosci.*, 9, 106–110, https://doi.org/10.1038/ngeo2630.
- Rossow, W. B., and R. A. Schiffer, 1999: Advances in understanding clouds from ISCCP. *Bull. Amer. Meteor. Soc.*, **80**, 2261–2288, https://doi.org/10.1175/1520-0477(1999)080<2261: AIUCFI>2.0.CO;2.
- Smirnov, D., and D. J. Vimont, 2012: Extratropical forcing of tropical Atlantic variability during boreal summer and fall. *J. Climate*, 25, 2056–2076, https://doi.org/10.1175/JCLI-D-11-00104.1.
- Tanimoto, Y., and S. P. Xie, 2002: Inter-hemispheric decadal variations in SST, surface wind, heat flux and cloud cover over the Atlantic Ocean. *J. Meteor. Soc. Japan*, 80, 1199–1219, https://doi.org/10.2151/jmsj.80.1199.
- Timmermann, A., and Coauthors, 2018: El Niño–Southern Oscillation complexity. *Nature*, 559, 535–545, https://doi.org/10.1038/s41586-018-0252-6.
- Vimont, D. J., D. S. Battisti, and A. C. Hirst, 2001: Footprinting: A seasonal connection between the tropics and mid-latitudes. *Geophys. Res. Lett.*, 28, 3923–3926, https://doi.org/10.1029/2001GL013435.
- —, and —, 2003a: The seasonal footprinting mechanism in the CSIRO general circulation models. *J. Climate*, **16**,

- 2653-2667, https://doi.org/10.1175/1520-0442(2003)016<2653: TSFMIT>2.0.CO;2.
- —, J, M. Wallace, and D. S. Battisti, 2003b: The seasonal footprinting mechanism in the Pacific: Implications for ENSO. *J. Climate*, 16, 2668–2675, https://doi.org/10.1175/1520-0442(2003) 016<2668:TSFMIT>2.0.CO;2.
- —, M. Alexander, and A. Fontaine, 2009: Midlatitude excitation of tropical variability in the Pacific: The role of thermodynamic coupling and seasonality. *J. Climate*, 22, 518–534, https://doi.org/10.1175/2008JCLI2220.1.
- Wu, X., Y. M. Okumura, and P. N. DiNezio, 2019: What controls the duration of El Niño and La Niña events? *J. Climate*, 32, 5941–5965, https://doi.org/10.1175/JCLI-D-18-0681.1.
- —, C. Deser, and P. N. DiNezio, 2021: Two-year dynamical predictions of ENSO event duration during 1954–2015.
 J. Climate, 34, 4069–4087, https://doi.org/10.1175/JCLI-D-20-0619.1.
- Xie, S.-P., 1999: A dynamic ocean–atmosphere model of the tropical Atlantic decadal variability. J. Climate, 12, 64–70, https://doi.org/10.1175/1520-0442-12.1.64.
- —, and S. G. H. Philander, 1994: A coupled ocean–atmosphere model of relevance to the ITCZ in the eastern Pacific. *Tellus*, 46A, 340–350, https://doi.org/10.1034/j.1600-0870.1994.t01-1-00001.x.
- —, C. Deser, G. A. Vecchi, J. Ma, H. Teng, and A. T. Wittenberg, 2010: Global warming pattern formation: Sea surface temperature and rainfall. *J. Climate*, 23, 966–986, https://doi.org/10.1175/2009JCLI3329.1.
- Yu, J. Y., and S. W. Fang, 2018: The distinct contributions of the seasonal footprinting and charged–discharged mechanisms to ENSO complexity. *Geophys. Res. Lett.*, 45, 6611–6618, https:// doi.org/10.1029/2018GL077664.
- Yuan, T., L. Oreopoulos, M. Zelinka, H. Yu, J. R. Norris, M. Chin, S. Platnick, and K. Meyer, 2016: Positive low cloud and dust feedbacks amplify tropical North Atlantic multidecadal oscillation. *Geophys. Res. Lett.*, 43, 1349–1356, https://doi.org/10.1002/2016GL067679.
- Zhang, Y., W. B. Rossow, A. A. Lacis, V. Oinas, and M. I. Mishchenko, 2004: Calculation of radiative fluxes from the surface to top of atmosphere based on ISCCP and other global data sets: Refinements of the radiative transfer model and the input data. *J. Geophys. Res.*, 109, D19105, https://doi.org/10.1029/2003JD004457.
- Zheng, X. T., C. Hui, and S. W. Yeh, 2018: Response of ENSO amplitude to global warming in CESM large ensemble: Uncertainty due to internal variability. *Climate Dyn.*, **50**, 4019–4035, https://doi.org/10.1007/s00382-017-3859-7.